Computing of cavitation characteristic and sensitivity curves for Francis pump-turbine

Lecturer dr. eng. ANTON IOSIF, Prof. dr. eng. IOAN SÂRBU
Department of Building Services
"Politehnica" University of Timisoara
Piata Bisericii, no. 4A, 300233 Timisoara
ROMANIA
ioan.sarbu@ct.upt.ro, anton.iosif@ct.upt.ro

Abstract: It is well known, that the fluid motion in reversible hydraulic machinery elements is a complex three-dimensional problem. In this paper it is developed an explicit numerical model based on Finite Element Method and Dual Reciprocity Method for the simulation of the flow velocity and pressure distributions on blade of the Francis type reversible radial-axial hydraulic machine's runner, in the hypothesis of ideal incompressible fluid and the relative rotational motion. The proposed numerical model was applied for reversible radial–axial hydraulic machinery operating as a pump. The blade has the basic profile NP205. This profile has a quadratic equation which defines its skeleton and its thickness function is that of a NACA profile with a maximum relative thickness of five percent. The numerical results for different discharge values have finally allowed obtaining the cavitation characteristic and sensitivity curves for the reversible hydraulic machinery.

Key-Words: Reversible hydraulic machines, Axial-symmetrical motion, Radial-axial profile cascades, Velocity and pressure distributions, Two-dimensional numerical model, Computer programs, Cavitation characteristic, Cavitation sensitivity curves.

1 Introduction

At it is well known, when fluid motion in the reversible hydraulic machinery elements is a complex three–dimensional problem [2], [9], [13], [14], [17].

Calculations of three-dimensional flow in rotating and stationary blade passages of turbomachinery are approximated by assuming that the three–dimensional flows can be represented by separate, nearly orthogonal, two–dimensional flows [1].

According to the authors, the Finite Element Method (FEM) and the Dual Reciprocity Method (DRM) allows the transformation of the three–dimensional problem of fluid motion in the reversible hydraulic machines (pump–turbines) runner in to a simpler two–dimensional problem, in the hypothesis of ideal incompressible fluid. For this purpose the following stages are recommended:

a) The axisymmetric potential motion is solved for a given domain that permites the determination of the hydrodinamic field and also the velocity and pressure distributions along the streamlines using FEM.

b) It is studied the fluid motion around radial-axial profile cascades disposed on the stream surfaces using DRM.

For solving both two–dimensional problems we consider the hypotheses:

– the fluid is inviscid and incompressible;
– mass forces are neglectable;
– the absolute motion is potential and stationary;
– the runner's number of rotations is constant;
– the motion is considered axial-symmetrical in the absence of runner blades;
– the stream surfaces are revolving surfaces;
– the motion is uniform at half of the cascade spacing upstream and respectively downstream of the cascade.

The relative fluid motion around radial–axial profile cascades is rotational. In order to determine this motion, the conformal mapping of the domain on the stream surface in an associated plane was used as well shown by Abdallah S. [1] and Carte I.N. [6].

The crossing of the stream surface with the runner blades generates a radial–axial cascade of profiles. Because the stream surface is deployble into a plane surface it is conformally mapped into an associated plane (Prasil) and the radial–axial cascade in a linear on. The determination of the motion in this plane was made by solving a boundary – value problem for the differential equation for the stream function ψ^*, obtaining the velocity and pressure field in the associated plane. Next, the results were transposed to the stream surface.

The numerical model was applied to the pump radial–axial cascade presented in [10]. The NP205 profile which is part of the blade's structure has a skeleton made of quadratic polynom and a four digit NACA profile thicknes functions.

2 Numerical model

2.1 Solving the fluid axial-symmetrical motion through pump-turbine runner

The paper presents a method of solving the potential axial-symmetrical motion of the inviscid incompressible fluid through the no blade runner of the reversible hydraulic machine functioning as a pump. Because of the axial-symmetrical nature of the motion, the use of a cylindrical coordinate system like (R, θ, Z) is in order.

From the previous hypotheses we know that the axial-symmetrical motion is a potential one, that means $\nabla \times \vec{v} = 0$, where $\vec{v} = \nabla \varphi$. Potential φ of velocity $\vec{v}$ is stationary ($\partial\varphi/\partial t = 0$) because the absolute motion is considered stationary ($\partial \vec{v} / \partial t = 0$).

Taking into acount that the fluid is incompressible ($\nabla \cdot \vec{v} = 0$) the Stokes equations are obtained:

– with the velocity potential φ:

$$\frac{\partial^2 \varphi}{\partial Z^2} + \frac{\partial^2 \varphi}{\partial R^2} + \frac{1}{R}\frac{\partial \varphi}{\partial R} = 0 \quad (1)$$

– with the stream function Ψ:

$$\frac{\partial^2 \Psi}{\partial Z^2} + \frac{\partial^2 \Psi}{\partial R^2} - \frac{1}{R}\frac{\partial \Psi}{\partial R} = 0 \quad (2)$$

because $\vec{v}$ and φ do not dependent on θ and: $\vec{v} = -\frac{\vec{i}_\theta}{R} \times \nabla\Psi$, $\nabla \times \vec{v} = 0$ and $\frac{\partial \Psi}{\partial \theta} = 0$.

The components of velocity $\vec{v}$ are given by the formulations:

$$v_Z = \frac{\partial \varphi}{\partial Z}; \quad v_R = \frac{\partial \varphi}{\partial R} \quad (3)$$

respectively:

$$v_Z = \frac{1}{R}\frac{\partial \Psi}{\partial R}; \quad v_R = -\frac{1}{R}\frac{\partial \Psi}{\partial Z} \quad (4)$$

The authors achieve solving the problem with Dirichlet and Neumann boundary conditions for the stream function Ψ, by means of integrating equation (2) using FEM.

In order to generalize the problem it is useful to take a dimensionless approach in the stream function, using the following variable interchange:

$$Z^* = Z L_{ax}^{-1}; \quad R^* = R L_{ax}^{-1} \quad (5)$$

and of function

$$\Psi^* = 2\pi Q^{-1} \Psi \quad (6)$$

where L_{ax} is the axial extension of the analysis domain, Q – discharge equal to $2\pi(\Psi - \Psi_0)$ and the value of Ψ_0 is equal to zero.

In this case, the Stokes equation for the stream function Ψ^* is written as such:

$$\frac{\partial^2 \Psi^*}{\partial Z^{*2}} + \frac{\partial^2 \Psi^*}{\partial R^{*2}} - \frac{1}{R^*}\frac{\partial \Psi^*}{\partial R^*} = 0 \quad (7)$$

and the dimensionless components of velocity v^* are given by:

$$v^*_{Z^*} = \frac{1}{R^*}\frac{\partial \Psi^*}{\partial R^*}; \quad v^*_{R^*} = -\frac{1}{R^*}\frac{\partial \Psi^*}{\partial Z^*} \quad (8)$$

The equations which express the connection between the velocity dimensionless components and the dimensional ones are written as follows:

$$v^*_{Z^*} = 2\pi L_{ax}^2 Q^{-1} v_Z; \quad v^*_{R^*} = 2\pi L_{ax}^2 Q^{-1} v_R \quad (9)$$

Because the problem to be solved requires mixed limit conditions, figure 1 show the geometric shape of the analysis domain and the limit conditions on its boundary for both the dimensional and the dimensionless approach.

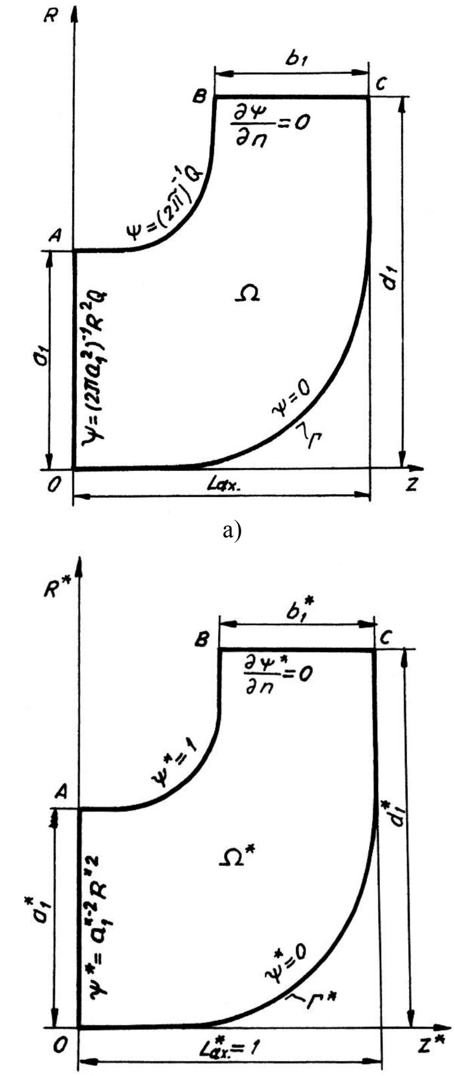

Fig.1 Analysis domain and the limit conditions for the dimensional case (a) and the dimensionless one (b)

Function Ψ^* is globally approximated on Ω^* as follows:

$$\Psi^* = a_\alpha^* \Psi_\alpha^*; \quad \alpha = 1,...,NG \tag{10}$$

where: NG representes the number of global nodes on domain Ω^*, resulted from its discretization in finite elements; a_α^* – global interpolation functions on Ω^*; Ψ_α^* – value of Ψ^* in global node α.

The Galerkin method is applied as follows [7]:

$$\int_{\Omega^*} \left(\frac{\partial^2 \Psi^*}{\partial {Z^*}^2} + \frac{\partial^2 \Psi^*}{\partial {R^*}^2} - \frac{1}{R^*} \frac{\partial \Psi^*}{\partial R^*} \right) a_\alpha^* \, d\Omega^* = 0 \tag{11}$$

Domain Ω^* is axial-symmetrical and thus $d\Omega^* = R^* \, d\theta \, dZ^* \, dR^*$. Using integration by parts on equation (11), a system of linear equations is obtained in its global form:

$$D_{\alpha\beta}^* \Psi_\beta^* = F_\alpha^*; \quad \alpha, \beta = 1,...,NG \tag{12}$$

where coefficients $D_{\alpha\beta}^*$ are written:

$$D_{\alpha\beta}^* = \int_{\Omega^*} \left(\frac{\partial a_\alpha^*}{\partial Z^*} \frac{\partial a_\beta^*}{\partial Z^*} + \frac{\partial a_\alpha^*}{\partial R^*} \frac{\partial a_\beta^*}{\partial R^*} \right) d\Omega^* + $$

$$+ 2 \int_{\Omega^*} {R^*}^{-1} a_\alpha^* \frac{\partial a_\beta^*}{\partial R^*} d\Omega^* \tag{13}$$

and for the free terms we have relation:

$$F_\alpha^* = \int_{\Gamma^*} \left(\frac{\partial \Psi^*}{\partial Z^*} n_{Z^*}^* + \frac{\partial \Psi^*}{\partial R^*} n_{R^*}^* \right) a_\alpha^{**} d\Gamma^* \tag{14}$$

where: a_β^* are the global interpolation functions on Ω^*; Ψ_β^* – value of Ψ^* in global node β; a_α^{**} – global interpolation functions on Γ^*; $n_{Z^*}^*$, $n_{R^*}^*$ – cosinus of the angle between normal n^* to Γ^* boundary and axis OZ^*, respectively OR^*.

Obtaining the global system of equations implies the knowledge of the finite element equation. The analysis domain has been discretized into a number E of isoparametric linear finite elements Ω^{*e} with boundary Γ^{*e}.

Function Ψ^* is approximated locally on each finite element as such:

$$\Psi^{*e} = a_N^* \Psi_N^{*e}; \quad N = 1,...,NL \tag{15}$$

in which: a_N^{*e} are the local interpolation functions; Ψ_N^{*e} – value of Ψ^{*e} in the local node N; $NL = 4$ – number of local nodes on Ω^{*e}.

If we apply the Galerkin method for the finite element we have the form of the local finite element equation:

$$D_{NM}^{*e} \Psi_M^{*e} = F_N^{*e}; \quad N, M = 1,...,NL \tag{16}$$

where coefficients D_{NM}^{*e} and the free terms F_N^{*e} are computed with the following relations:

$$D_{NM}^{*e} = \int_{\Omega^{*e}} \left(\frac{\partial a_N^{*e}}{\partial Z^*} \frac{\partial a_M^{*e}}{\partial Z^*} + \frac{\partial a_N^{*e}}{\partial R^*} \frac{\partial a_M^{*e}}{\partial R^*} \right) d\Omega^{*e} + $$

$$+ 2 \int_{\Omega^{*e}} {R^*}^{-1} a_N^* \frac{\partial a_M^{*e}}{\partial R^*} d\Omega^{*e} \tag{17}$$

$$F_N^{*e} = \int_{\Gamma^{*e}} \left(\frac{\partial \Psi^{*e}}{\partial Z^*} n_{Z^*}^* + \frac{\partial \Psi^{*e}}{\partial R^*} n_{R^*}^* \right) a_N^{**e} d\Gamma^{*e} \tag{18}$$

The coefficients D_{NM}^{*e} are numerically evaluated using a Gauss quadrature formula [10]:

$$D_{NM}^{*e} = 32^{-1} \sum_{i=1}^{n} \sum_{j=1}^{n} w_i w_j f_{NM}(\zeta_i, \eta_j) \tag{19}$$

where: n is the number of Gauss integration points from inside the finite element; ζ_i and η_j – natural coordinates of the integration point; w_i, w_j – weight factors.

Taking into account the limit conditions for the stream function, the free terms F_N^{*e} are equal to zero on Γ^{*e}, respectively Γ^*. Knowing the local values of Ψ_N^{*e}, D_{NM}^{*e}, F_N^{*e}, allows the computation of the global values with the help of Boolean matrices:

$$\Psi_\alpha^* = \sum_{e=1}^{E} \Delta_{N\alpha}^{e} \Psi_N^{*e}$$

$$D_{\alpha\beta}^* = \sum_{e=1}^{E} D_{NM}^{*e} \Delta_{N\alpha}^{e} \Delta_{M\beta}^{e} \tag{20}$$

$$F_\alpha^* = \sum_{e=1}^{E} F_N^{*e} \Delta_{N\alpha}^{e}$$

where $\Delta_{N\alpha}^{e}$, $\Delta_{M\beta}^{e}$ are the elements of Boolean matrix Δ^e which has dimensions $NL \times NG$.

The components of velocity v^{*e} on the finite element are computed in the gravity center of the finite element (for $\zeta = 0$, $\eta = 0$) using the relations [7], [8]:

$$\begin{aligned} v_{Z^*}^{*e} &= 4\alpha_0^{-1} a_2^{-1} A_{N2} \Psi_N^{*e} \\ v_{R^*}^{*e} &= -4\alpha_0^{-1} a_2^{-1} A_{N1} \Psi_N^{*e} \end{aligned} \tag{21}$$

and the velocity´s value v^* in nodes is computed using the arithmetical average of the components pertaining to the neighbouring finite elements:

$$v^* = \left(v_{Z^*}^{*2} + v_{R^*}^{*2} \right)^{\frac{1}{2}} \tag{22}$$

Knowing the components of velocity v^* in the global nodes, we can compute the values of φ^* in these nodes by use of the following equation:

$$\varphi^* = \varphi_0^* + \int_c v_{Z^*}^* dZ^* + v_{R^*}^* dR^* \qquad (23)$$

imposing $\varphi_0^* = 0$ on BC.

The authors have developed a computer program in the FORTRAN programming language for IBM-PC compatible microsystems. Using this porogram is obtained the hydrodynamic field (fig. 2) defined by the streamlines Ψ^* = const. and the lines of equal potential φ^* = const. also the velocity (fig. 3) and pressure distributions (fig. 4) along the streamlines, considering the following data: L_{ax} = 2.027 m, $a_1^* = 0.666$, v^{AB} = 12.61 m/s.

Velocity $\overline{v}^*$ corresponding to a point on the streamline represents the ratio between two dimensionless velocities:

$$\overline{v}^* = \frac{v^*}{v^{*AB}} \qquad (24)$$

where:

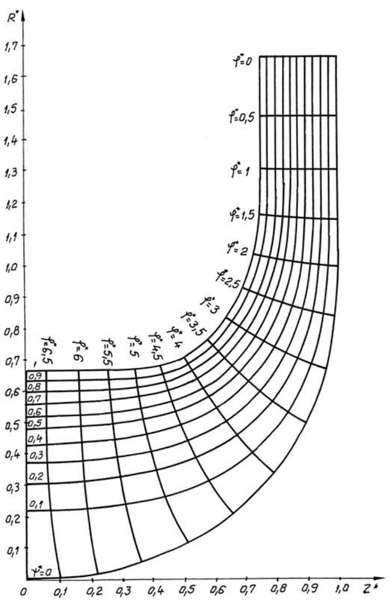

Fig. 2 Hydrodynamic field

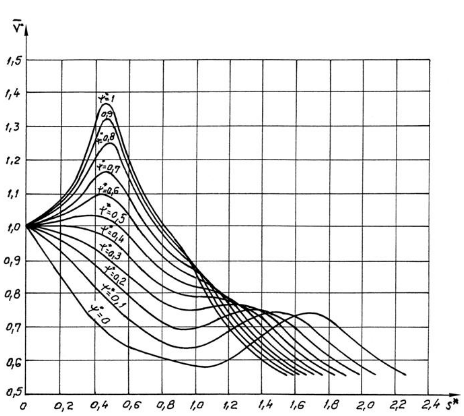

Fig. 3 Velocity distributions along the stramlines

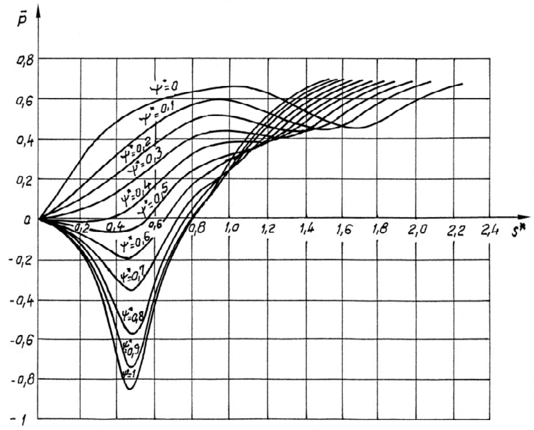

Fig. 4 Pressure distributions along the stramlines

$$v^{*AB} = 2(a_1^*)^{-2} = 4.5 \qquad (25)$$

in which a_1^* is the dimensionless radius coresponding to the entry in the considered runner (fig. 1-b). Dimensionless velocity v for every streamline point is obtained by multiplying $\overline{v}^*$ by v^{AB}.

In order to obtain the pressure distribution along the streamlines (fig. 4) the equation below is used:

$$\overline{p} = 1 - \overline{v}^{*2} \qquad (26)$$

Relation (26) is result of Bernoulli´s theoreme for the potential stationary motion, written for two streamline points one belonging to the AB boundary and the other is the current one.

From figures 3 and 4 we can identify the maximum value point for $\overline{v}^*$ and the minimum value for $\overline{p}$. We notice that for Ψ^* = 1 we obtain $\overline{v}_{\max}^* = 1.364$ and $\overline{p} = -0.86$ for $s^* = 0.46$ the value of the streamline curve arch. This means that here exists a higher probability to produce cavitational phenomenon.

For solving the rotational motion on the stream surface we shall retain only the stream-lines from the hydrodynamic field in the meri-dian plane and in this plane (fig. 5) we shall put the entry edge and the exit edge of the blade, the latter being parallel to axis OZ^*, and is found at radius $R_P^* = 1.233$.

2.2 Basis of the Dual Reciprocity Method

The DRM proposed by Brebbia A. and Nardini D. [5], [15], and developed by Novak A., Partridge P. and Wrobel L. [18], [19], has as an objective the transformation of domain integrals into boundary integrals, which shows it is based on the BEM.

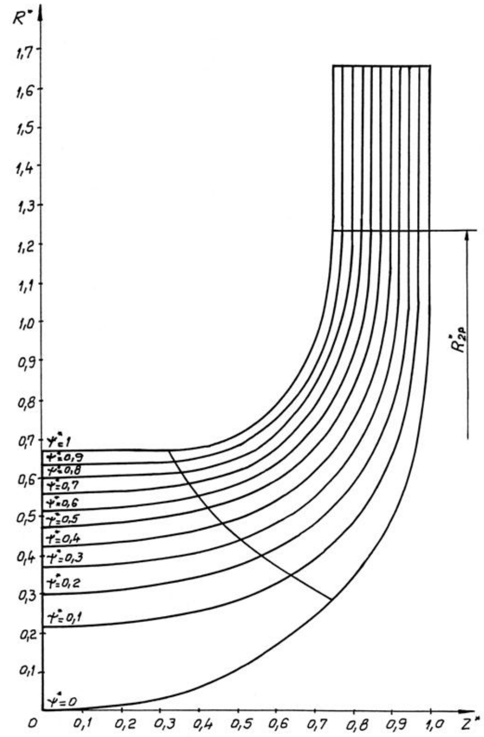

Fig. 5 The streamlines and entry and exit edges for the runner blades

The elements that constitute the basis of the method are applied to equations as such:

$$\nabla^2 u = -b \tag{27}$$

where b is one or more dependent functions of (x, y, u, t) or of (x, y, u), when t (time) is missing. Solution u to equation (27) can be obtained from solution $\breve{u}$ out of the Laplace equation and a particular solu-tion $\hat{u}$ as follows:

$$u = \breve{u} + \hat{u} \tag{28}$$

In [19] it is proposed to use a limited series of particular solutios and for b the relation:

$$b = \sum_{j=1}^{N+L} F_j \alpha_j \tag{29}$$

where F_j is the function associated to point j and α_j are the $\boldsymbol{\alpha}$ vector elements. Because we have N boundary nodes and L internal nodes from Ω domain, as presentated in figure 6, we have as a result N+L values for F_j and $\boldsymbol{\alpha}$.

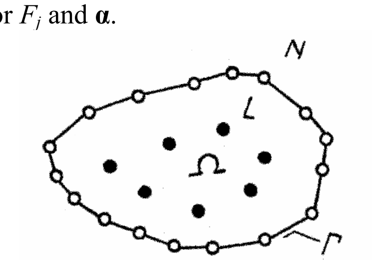

Fig. 6 Boundary and internal nodes from Ω domain

Starting with the basic equation:

$$\nabla^2 u = -\sum_{j=1}^{N+L} (\nabla^2 \hat{u}_j)\alpha_j \tag{30}$$

to whch we apply the usual BEM technique, after then Γ boundary's discretization in linear elements, the following matrix equation insues:

$$\mathbf{Hu} - \mathbf{Gq} = (\mathbf{G}\hat{\mathbf{Q}} - \mathbf{H}\hat{\mathbf{U}})\boldsymbol{\alpha} \tag{31}$$

where **u**, **q** are the solution vectors and of its normal derivative of N+L size, and matrices **H**, **G**, $\hat{\mathbf{Q}}$, $\hat{\mathbf{H}}$, have the size (N+L)×(N+L). For computing matrix elements $\hat{\mathbf{Q}}$, $\hat{\mathbf{H}}$ a limited serier of particular solution $\hat{u}$ is proposed and its normal derivative $\hat{q}$, where the distance function ***r*** intervenes:

$$\begin{aligned} \hat{u} &= \frac{r^2}{4} + \frac{r^3}{9} + ... + \frac{r^{m+2}}{(m+2)^2} \\ \hat{q} &= -\left(\bar{x}\frac{\partial x}{\partial n} + \bar{y}\frac{\partial y}{\partial n}\right)\left(\frac{1}{2} + \frac{r}{3} + ... + \frac{r^m}{m+2}\right) \end{aligned} \tag{32}$$

The calculus of elements H_{ij} and G_{ij} corresponding to matrices **H** and **G** is the same as for linear boundary elements.

The matrix equation (31), after implementing the limit conditions leads to a linear system of N+L equations with N+L unknows, these being the values of function u and its normal derivative q in the nodes where they are unknown.

2.3 Equation for relative rotational motion on the stream surface

The fluid flow in a Francis type runner is considered nonviscous and incompressible. The crossing of the stream surface with the runner blades in functioning as a pump will determine a radial-axial cascade with profiles represented in figure 7.

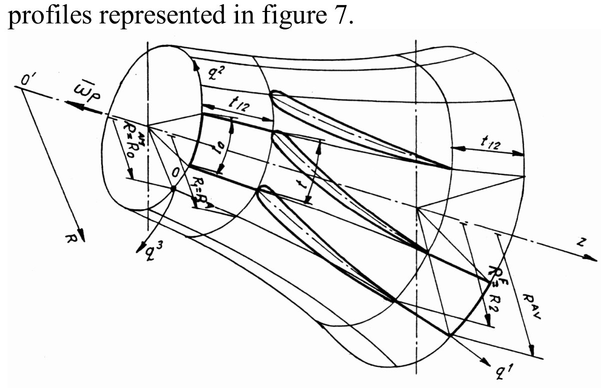

Fig. 7 Radial-axial cascade on the stream surface

If we consider the relation between the absolute velocity v, the relative velocity w and u which represents the peripheral velocity, the absolute motion of the ideal fluid being considered potential as well as introducing the $Oq^1q^2q^3$ orthogonal curvelinear coordonate system will lead to the obtaining of the stream surface motion equation [10]:

$$\frac{\partial}{\partial q^1}\left[R R_0^{-1} w_{(2)}\right] - \frac{\partial w_{(1)}}{\partial q^2} + R_0^{-1} R f_P = 0 \qquad (33)$$

where:

$$f_P = 2\omega_P \frac{dR}{dz}\left[1+\left(\frac{dR}{dz}\right)^2\right]^{-\frac{1}{2}} \qquad (34)$$

in which: $w_{(1)}$, $w_{(2)}$ are the relative flow velocity components of the motion on the stream surface, ω_P the angular velocity, R_0 the radius coresponding to the origin of curvelinear coordinates system, and z, R the axial cordinates and radius, variables in the case of the axisymmetric motion.

2.4 Conformal mapping of the radial-axial cascade

Because equation (33) is not useful for the numerical calculation, there is a need for the following change of variables (x; y):

$$x = \int_0^{q^1} R_0 R^{-1} dq^1; \quad y = q^2 \qquad (35)$$

The equations (35) realise the geometric transformation of the stream surface in the associated plane and of the radial-axial cascade into a linear one. In numerical computation accomplished in associated plane where the linear cascade is found, as shown in figure 8 are used the following dimensionless variables:

$$\bar{x}^* = \frac{x^*}{L^*}; \quad \bar{y}^* = \frac{y^*}{L^*} \qquad (36)$$

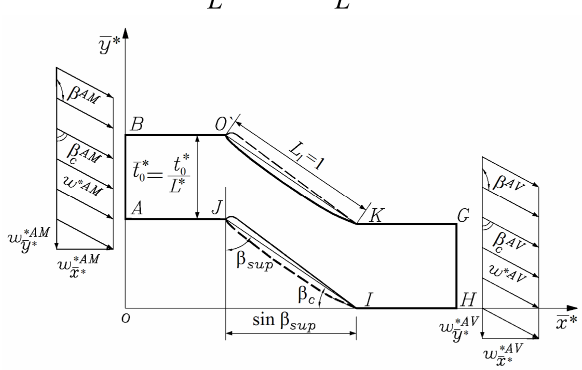

Fig. 8 Analysis domain from the associated plane

where:

$$x^* = \int_{s_0^*}^{s^*} r_0^* r^{*-1} ds^*; \quad y^* = r_0^* \theta \qquad (37)$$

$$r_0^* = \frac{R_0}{L_{ax}}; \quad r^* = \frac{R}{L_{ax}} \qquad (38)$$

in which: s_0^* is the dimensionless arc coresponding to the origin O (Fig. 7), L_{ax} the dimensional axial extension of the analysis domain, and L^* the length of cascade chord in the associated plane obtained through the dimensionlles way of deeling with problem in the stream function Ψ^* solved of the axisymmetric motion.

2.5 Solving the dimensionless differential equation for stream function in associated plane

In the associated plane, taking into account equation (33) it has been deduced the following differential dimensionless equation for the ψ^* stream function in this plane:

$$\frac{\partial^2 \psi^*}{\partial \bar{x}^{*2}} + \frac{\partial^2 \psi^*}{\partial \bar{y}^{*2}} - \frac{1}{h(\bar{x}^*)}\frac{dh(\bar{x}^*)}{d\bar{x}^*}\frac{\partial \psi^*}{\partial \bar{x}^*} - h(\bar{x}^*)\left(r_0^{*-1} r^*\right)^2 f_P^* = 0 \qquad (39)$$

where:

$$f_P^* = 2\omega_P^* \frac{dr^*}{dz^*}\left[1+\left(\frac{dr^*}{dz^*}\right)^2\right]^{-\frac{1}{2}} \qquad (40)$$

and $h(\bar{x}^*)$ is thickness function of the variable fluid layer.

Differential equation (39) is solved with the DRM, if we take into acount the analysis domain shown in figure 8 and the following boundary conditions:

$$\begin{aligned}
&\psi^* = 0 \quad \text{on JI} \\
&\psi^* = \bar{t}_0^* \quad \text{on O'K} \\
&\frac{\partial \psi^*}{\partial \bar{n}^*} = ctg\beta^{AM} = -ctg\beta_c^{AM} \quad \text{on AB} \\
&\frac{\partial \psi^*}{\partial \bar{n}^*} = -ctg\beta^{AV} = ctg\beta_c^{AV} \quad \text{on HG} \\
&\psi^* = \psi^*_{AJ,IH} + \bar{t}_0^* \quad \text{on BO', KG} \\
&\frac{\partial \psi^*}{\partial \bar{n}^*} = -\left(\frac{\partial \psi^*}{\partial \bar{n}^*}\right)_{AJ,IH} \quad \text{on BO', KG}
\end{aligned} \qquad (41)$$

where: $\bar{t}_0^*$ is the cascade step from associated plane, $\bar{n}^*$ the external normal to boundary, and β the angle between relative and peripheral velocity.

Equation (39) can be written like so:

$$\nabla^2 \psi^* = b \qquad (42)$$

where b is the sum of two terms:

$$a = h(\bar{x}^*)\left(r_0^{*-1} r^*\right)^2 f_P^*; \quad c = \frac{h'(\bar{x}^*)}{h(\bar{x}^*)} \frac{\partial \psi^*}{\partial \bar{x}^*} \tag{43}$$

If we take into account DRM we have for (39) the following matrix equation:

$$\mathbf{H}\boldsymbol{\psi}^* - \mathbf{G}\mathbf{q} = (\mathbf{H}\hat{\mathbf{U}} - \mathbf{G}\hat{\mathbf{Q}})(\boldsymbol{\alpha} + \boldsymbol{\lambda}) \tag{44}$$

in which $\boldsymbol{\alpha}$, $\boldsymbol{\lambda}$ are vectors determined as such:

$$\boldsymbol{\alpha} = \mathbf{F}^{-1}\mathbf{a}; \quad \boldsymbol{\lambda} = \mathbf{F}^{-1}\mathbf{c} \tag{45}$$

In the above equation **a**, **c** are vectors, and $\mathbf{F}^{-1}$ is reciprocal of matrix **F**. Solving matrix equation (44) with the boundary conditions (41) is done through a repetitiv process, starting with the Lplace equation solution. The results from the plane are transposed on the stream surface using the relations below:

$$\bar{w}_{(\,)} = R_0 R^{-1} \bar{w}^* \tag{46}$$

$$\bar{p}_{(\,)} = 1 - \left(R_0 R^{-1}\right)^2 \bar{w}^{*2} + \omega_P{}^2 R_0^2 \times \\ \times \left(v_{m0} w^{*AM}\right)^{-2} \left[\left(R R_0^{-1}\right)^2 - 1\right] \tag{47}$$

obtaining the velocity and pressure distributions ($\bar{w}_{(\,)}$, $\bar{p}_{(\,)}$) on the profile from the radial–axial cascade, namely on the reversible runner blades. The dimensionless velocity $\bar{w}^*$ has the expresion:

$$\bar{w}^* = \frac{w^*}{w^{*AM}} \tag{48}$$

where: w^* is the dimensionless velocity computed in the associated plane, w^{*AM} – dimensionless velocity upward the linear cascade, v_{m0} – dimensional meridional velocity corresponding to the "O" origin of the curvelinear coordinate system.

A computer program has been elaborated on the basis of the numerical model developed. It was realized in the FORTRAN programming language, for IBM-PC compatible microsystems.

3 Results of numerical model application to a pump-turbine

The proposed computational model was applied for a reversible radial–axial hydraulic machinery functioning as a pump which following fundamental characteristics: H_P=317 m, Q_P=72.35 m^3/s, P_P=250 MW, η_P = 0.9, n_{sp} = 130, n_P = 300 rpm, L^* = 1.476, β^{AM} = 159°, β_c^{AM} = 21°, β^{AV} = 155°, β_c^{AV} = 25°, β_{sup} = 24°, β_c = 66°. The number of runner blades is Z_P = 7 and maximum relative thickness of profile is d/l = 0.5. Thickness function of the variable fluid layer is expressed as follow:

$$h\left(\bar{x}^*\right) = 57.74\bar{x}^{*5} - 81.38\bar{x}^{*4} + 38.67\bar{x}^{*3} - \\ - 7.27\bar{x}^{*2} - 0.17\bar{x}^* + 0.998 \tag{49}$$

For solving the matrix equation (43) the analysis domain is discretized on the boundary into linear elements, and the internal nodes are established [12]. The nummerical calculus is performed for $N = 43$ nodes of the boundary and $L = 20$ internal nodes.

The flow velocity and pressure distributions on the reversible runner blade are simulated with the computer program for the discharge Q_c = 72.35 m^3/s and the medium stream surface generated by the streamline Ψ^*=0.6 and represented in figures 9 and 10. This representation was made along the L^*_{LOX} dimensionless loxodrome. The same figures represent the velocity and pressure distributions computed also with FEM. From the representation of the velocity and pressure distributions (fig. 9, 10) we can ascertain the following values on the profile intrados using DRM: $\bar{w}_{(\,)}$=1.56, $\bar{p}_{(\,)}$= –1.17 and FEM: $\bar{w}_{(\,)}$=1.46 $\bar{p}_{(\,)}$= –1. It can be observed in general a good coordonaton of the values obtained with the two numerical methods.

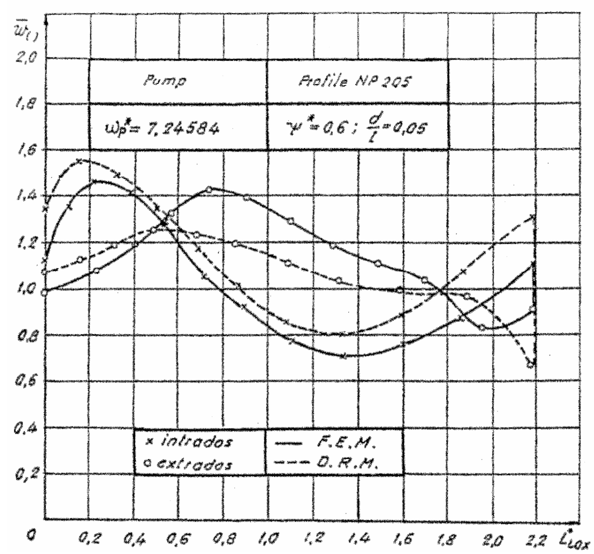

Fig. 9 Velocity distribution on the runner blade

4 Cavitation characteristic and sensitivity curves

The reversible hydraulic machine functions, in reality, at random discharge values Q_x that can differ or are equal to the computed discharge. Taking into account the unfavourable behaviour of the machine during pump regime than during the turbine regime [2], [3], it is necessary to determine the cavitation characteristic $\sigma_{Px} = f(Q_x/Q_c)$ and the cavitation sensitivity curves $k_{p\,\max,\,x} = f(Q_x/Q_c)$ from the very stage of designing the runner.

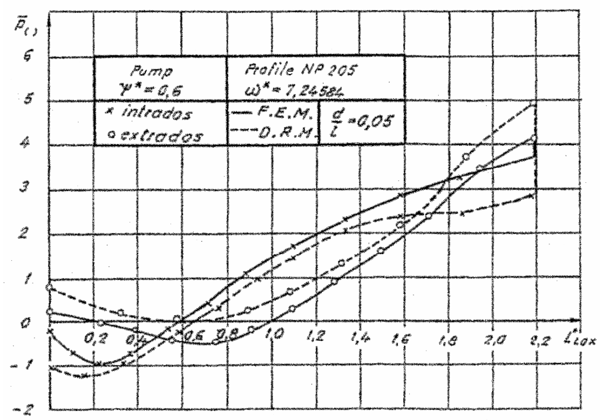

Fig. 10 Pressure distribution on the runner blade

These theoretical characteristics are determined based on the coefficient of minimal pressure distributions obtained for Q_x = [0.8, 1.0, 1.2, 1.4]×Q_c and Ψ^* = 0.6. Figure 11 presents the Francis pump-turbine hydraulic circulation while operating as a pump, and figure 12 shows the velocity triangles corresponding to points 0 on the stramlines at discharges Q_x.

In the case of Q_x random discharge regimes, velocity (fig. 13) and pressure (fig. 14) distributions were obtained using DRM, one the blade of the reversible hydraulic machine.

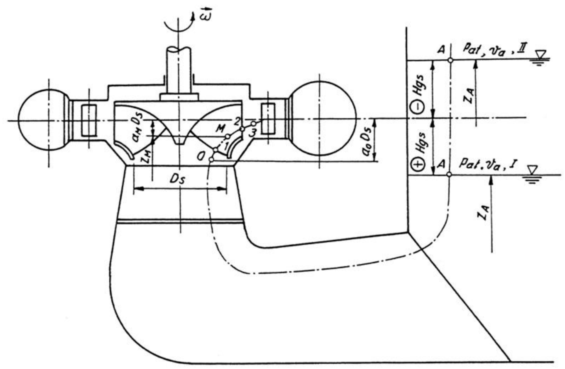

Fig. 11 Hydraulic ciculation of reversible machine operating as a pump

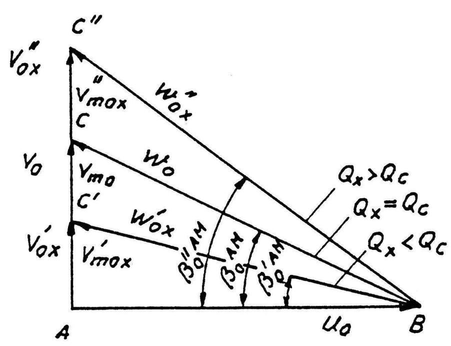

Fig. 12 Velocity triangles corresponding to point 0

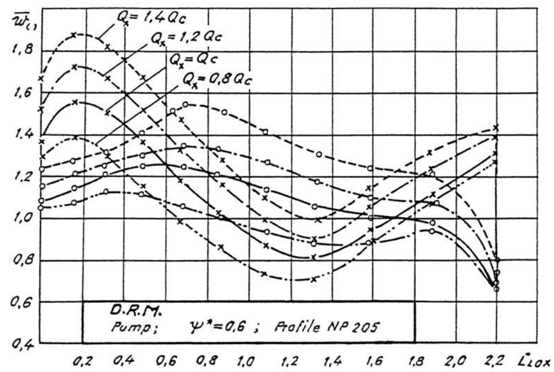

Fig. 13 Velocity distributions on the hydraulic machine´s blade

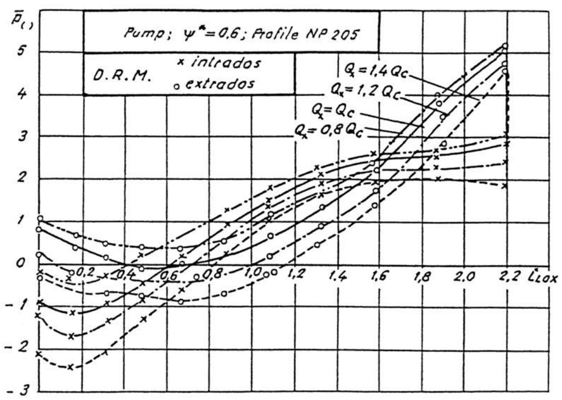

Fig. 14 Pressure distributions on the hydraulic machine´s blade

For computing the cavitation coefficient σ_{Px} for discharge Q_x, equation was employed:

$$\sigma_{Px} = k_{p\max,x}\frac{w_{0x}^2}{2gH_{Px}} - k_{ux}\frac{u_{0x}^2}{2gH_{Px}} + \frac{v_{0x}^2}{2gH_{Px}} + \\ + \frac{\sum h_{p0-Mx}}{H_{P_X}} + \frac{a_{Mx}D_S}{H_{Px}} \qquad (50)$$

where hydraulic losses $\sum h_{p0-Mx}$ are equal to zero for the inviscid incompressible fluid.

The pumping head H_{Px} is computed with relation:

$$H_{Px} = \frac{\eta_{hP}}{g(1+p)} u_{2P}\left(u_{2P} - \frac{Q_x}{\pi D_{2P} b_{2P}} ctg\beta_{2P}\right) \quad (51)$$

where: p is the influence coefficient for the finite number of blades Z_P, (Z_P = 7, p = 0.3836); η_{hP} = 0.96 – the hydraulic efficiency of the runner.

In relation (1) factor $k_{p\ \max,\ x}$ is equal to the value $-\overline{p}_{()\min,x}$ obtained from the pressure distributions for discharge Q_x, and the absolute velocity (v_{0x}), the relative velocity (w_{0x}) and the peripheral velocity (u_{0x}) corresponding to point 0 from figure 11, respectively to origine O of the curvelinear coordinate system $Oq^1q^2q^3$ from figure 7.

Results obtained with DRM allowed the illustration (fig. 15 and 16) of the cavitation characteristic and also the cavitation sensitivity curves compaired with the respective characteristics determined with FEM.

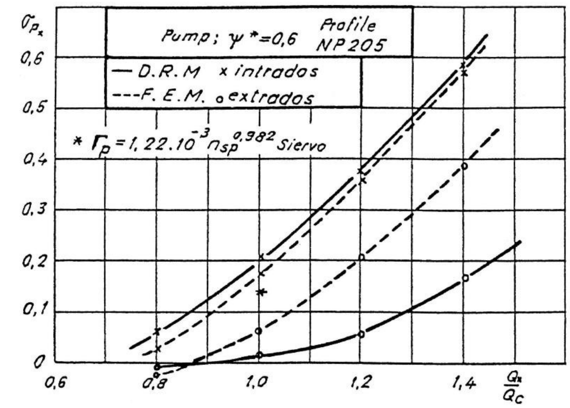

Fig. 15 Cavitation characteristic $\sigma_{Px} = f(Q_x/Q_c)$

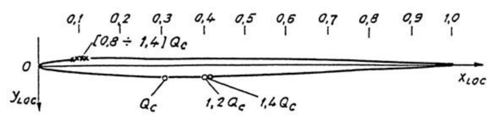

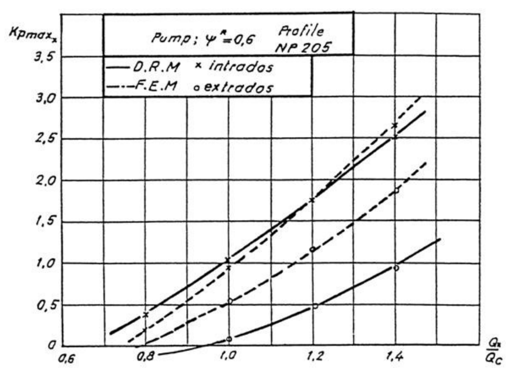

Fig. 16 Cavitation sensitivity curves $k_{p\,\max,x} = f(Q_x/Q_c)$

In figure 15 the value of σ_P equal to 0.145 was also written, which was obtained with the statistical equation recommended with Siervo F. [22] for $Q_x = Q_c = Q_P$. It can be noticed that this value is closer to the σ_P values computed with DRM and FEM for the intrados.

Figures 15 and 16 show that increasing discharge Q_x, leads to an increase in the values of σ_{Px} and $k_{p\,\max,\,x}$, thus leading to an unfavourable of the runner, from the cavitational point of view. These operating conditions are makeing possible the development of cavitation phenomenon inside the runner and decreasing the energy efficiency.

In the following, we proceed to present a method of computing the cavitation coefficient σ_{Px} and the location of point M in which the pressure equals the value of $\overline{p}_{()\min,x}$ for $\Psi^* = 0.6$ and $Q_x = Q_c = Q_P = 72.35$ m^3/s. For the case in which $Q_x/Q_c = 1$, relation (50) can be formulated as such:

$$\sigma_P = k_{p\max}\frac{w_0^2}{2gH_P} - k_u\frac{u_0^2}{2gH_P} + \frac{v_0^2}{2gH_P} + \frac{\sum h_{p0-M}}{H_P} + \frac{a_M D_S}{H_P} \tag{52}$$

where the peripheral velocity coefficient is given by:

$$k_u = \left(\frac{R_M}{R_0}\right)^2 - 1 = \left(\frac{R_M^*}{R_0^*}\right)^2 - 1 \tag{53}$$

and

$$a_M D_S = \left(0.8625 - Z_M^*\right)L_{ax.} \tag{54}$$

where radius R_M^* of point M and radius R_0^* of point 0 are dimensionless and $R_M = R_M^* L_{ax}$ and $R_0 = R_0^* L_{ax}$ are dimensional.

In equation (3) hydraulic losses $\sum h_{p0-M}$ are equal to zero, and the values for velocities are: $v_0 = 12.9$ m/s, $u_0 = 33.45$ m/s, $w_0 = 35.3$ m/s.

For establishing the location of point M, the following approximation polynomials have been determined:

$$\frac{1}{R^*} = 0.10827 s^{*6} - 1.5184 s^{*5} + 4.5641 s^{*4} - 3.809 s^{*3} + 0.27393 s^{*2} + 0.10227 s^* + 1.9152 \tag{55}$$

$$Z^* = 0.023713 s^{*5} + 0.27655 s^{*4} - 1.1190 s^{*3} + 0.80934 s^{*2} + 0.80887 s^* + 0.011191 \tag{56}$$

$$s^* = 0.53727 x^{*4} + 0.029893 x^{*3} + 0.02595 x^{*2} + 1.0012 x^* + 0.1624 \tag{57}$$

For $s^* = 0$ the result is $R_0^* = 0.522$ and the dimensionless abscissa of point M is given by relation:

$$x_M^* = L^* \overline{x}_M^* \tag{58}$$

in which $\overline{x}_M^*$ is the abscissa of point M in plane $\overline{y}^* o \overline{x}^*$.

The computation results are presented in table 1.

Table 1. The coordinates of point M's location

Method	$\overline{x}_M^*$	x_M^*	s_M^*	Z_M^*	R_M^*	k_u	σ_P
DRM	0.220	0.325	0.498	0.494	0.577	0.23	0.216
FEM	0.238	0.351	0.526	0.520	0.587	0.27	0.175

Figure 17 illustrates the location of point M obtained using the two nummerical methods DRM and FEM.

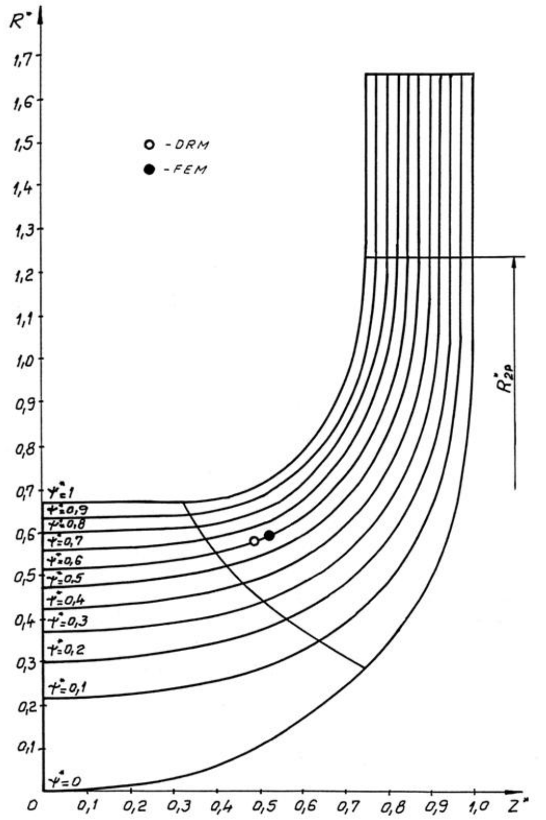

Fig. 17 Location of point *M*

We can see small differences between the results obtained with DRM and FEM, which can be explained by the computational errors generated while employing these methods.

Also we can notice that point *M* of minimal pressure is found in the close vecinity of the area where the liquid flow is on the blade of the hydraulic machine in a pumping state, which has been experimentally identifyed by Anton I. [3].

5 Conclusions

The authors show a method for solving a three–dimensional problem by transforming it into two problems both two–dimensional for determining the velocity and pressure distributions on the blade of the pump–turbine runner, accepting the fact that the fluid is inviscid.

For simulating the velocity and pressure distributions it is necessary to solve a mixt boundary conditions problem in the associated plane. For this purpose, a numerical computational model has been developed, with the help of DRM for solving the partial derivative equation (39) imposing Dirichlet and Neumann boundary conditions on the boundary of the analysis field in the associated plane. This is the novelty in solving the problem.

The modality of solving the problem we approached with DRM can be a starting point in the case of viscous fluid.

Theoretical study of the cavitation characteristic and sensitivity, and also establishing the location of the minimal pressure point, constitute important results for all the designing engineers in this field of expertise.

References:

[1] Abdallah, S. and Henderson, R.E. Improved approach to the streamline curveture method in turbomachiney, *ASME Journal of Fluids Engineering*, vol. 109, no. 3, 1987, pp.213-217.

[2] Anton, I. *Hydraulic turbines*, Facla Publishing House, Timisoara (in Romanian), 1979.

[3] Anton, I. *Cavitation*, Romanian Academy Publishing House, Bucharest (in Romanian), 1985.

[4] Arakawa, C. Matsuo, Y. and Kubota, T. Numerical simulation of Francis runner using pseudocompressibility, *Proceding of the 15th IAHR Symposium*, Belgrade, Yugoslavia, vol. C1, 1990, pp. 1-10.

[5] Brebbia, A.C. and Nardini, D. Dynamic analysis in solid mechanics by an alternative boundary element procedure, *International Journal of Soil Dynamics and Earthqurke*, vol. 2, no. 4, 1983. pp. 228-233.

[6] Carte, I.N. Determination of the incompressible fluid motion round radial–axial profile cascades through the finite element method, *Mécanique Appliquée*, Bucharest, Romania, tome 32, no.6, 1987, pp. 639-649.

[7] Carte, I.N. *Contributions to the study of radial-axial cascades and applicattions for francis turbines design*, PhD thesis, Polytechnic Institute „Traian Vuia" of Timişoara (in Romanian), 1986.

[8] Chung, T.J. *Finite Element Analysis in Fluids Dynamics*, Mc Graw–Hill, New York, 1978.

[9] Dring, R.P. Joslyn, H.D. Hardin, L.W. and Wagner, J.H. Turbine rotor–stator interaction, *ASME Journal of Engineering Power*, vol. 104, 1982, pp. 729-742.

[10] Iosif, A. *Radial–axial reversible hydraulic machinery*, PhD Thesis, „Politehnica" University of Timisoara, Timisoara (in Romanian), 1998.

[11] Iosif, A. and Sârbu, I. Simulation of axisymmetric motion in Francis reversible runner, *Proceedings of the 7th International Conference on Hydroscience and Engineering*, Philadelphia, USA, vol. 1, 2006, pp. 291-297.

[12] Iosif, A. and Sârbu, I. Simulation of velocities and pressures distribution on blade of turbine-runner, "*Continuum Mechanics, Fluids, Heat*", *Proceedings of the 7th WSEAS Int. Conference on Fluid Mechanics*, Cambridge, UK, February 23-25, 2010.

[13] Kolšek, T. Duhovnik, J. and Bergant, A. Simulation of unsteady flow and runner rotation during shutdown of an axial water turbine, *Journal of Hydraulic Research*, Madrid, Spain, vol. 44, no. 1, 2006, pp. 129-137.

[14] Naidu, B.S.K. Computerised design development and model testing of a high head Francis turbine runner, *Proceedings of the 15th IAHR Symposium*, Belgrade, Yugoslavia, vol. Q4, 1990, pp. 1-11.

[15] Nardini, D. and Brebbia, A.C. Boundary integral formulation of mass matrices for dynamic analysis, *Boundary Element Research*, vol.2, Springer–Verlag, Berlin and New York, 1985.

[16] Nouri, N.M. Eslamdoost, A. Shienejad, A. and Moghimi, M. Calculation of hydrodynamic drag force exerted on a supercavitating slender body using boundary element method, *WSEAS Transaction on Fluid Mechanics*, vol. 1, no. 6, 2006, pp. 566-571.

[17] Novac, R.A. and Hearsey, R.M. A nearly three–dimensional intrblade computing system for turbomachinery*, ASME Journal of Fluids Engineering*, vol. 99, no. 3, 1994, pp. 154-166.

[18] Novak, A.J. and Brebbia, A.C. The multiple reciprocity method: A new approach for transforming BEM domain integrals to the boundary, *Engineering Analysis,* vol. 6, no. 3, 1989, pp. 164-167.

[19] Partridge, W.P. Brebbia, A.C. and Wrobel, C.L. *The Dual Reciprocity Method*, Computational Mechanics Publication Sounthampton, Boston, Elsevier Applie Science London, New York, 1992.

[20] Partridge, W.P. and Brebbia, A.C. Computer implementation of the BEM Dual reciprocity method for the solution of general field equations, *Comunications Applied Numerical Methods*, vol. 6, no. 2, 1990, pp. 83-92.

[21] Peter, J. Marcelet, M. Comparison of surrogate models for turbomachinery design, *WSEAS Transaction on Fluid Mechanics*, vol. 3, no. 1, 2008, pp. 10-17.

[22] Siervo, F. Lugaresi, A. Modern trends in selecting and designing reversible Francis pump–turbines. *Water Power and Dam Construction*, May, 1980.

[23] Simoni, D. Ubaldi, M. Zunino, P. Von Karman vortices formation at the trailing edge of a turbine blade, *WSEAS Transaction on Fluid Mechanics*, vol. 3, no. 4, 2008, pp. 349-358.

[24] Schultz, J.L. *Modelisation de la cavitation partielle dans les pompes*, PhD thesis, Institut National Polytechnique de Grenoble, 1988.

[25] Timouchev, S.F. and Illichov, K.P. 2D numerical simulation of unsteady pressure field in centri-fugal pumps, *Proceedings of Int. INSE Symposium*, Lyon, France, vol. 3, 1995.

[26] Wrobel, C.L. and Brebbia, A.C. The dual reciprocity boundary element formulation for nonlinear diffusion problems, *Computer Methods in Applied Mechanics and Engineering*, vol. 65, no. 2, 1987, pp. 147-161.